Numerical and Experimental Study of an Industrial Case for Grain Size Evolution in Bainitic Steel in Controlled Hot Forging and its Influence on Mechanical Performance

T.M. Ivaniski[a]* , P.J. de Castro[a] , D. Rodrigues[a], J. Épp[b,c], R.M. Nunes[a] , A. da S. Rocha[a]

[a]Universidade Federal do Rio Grande do Sul, Departamento de Metalurgia, Centro de Tecnologia, Laboratório de Transformação Mecânica, Porto Alegre, RS, Brasil.
[b]Leibniz-Institut für Werkstofforientierte Technologien, Bremen, Germany.
[c]University of Bremen, MAPEX Centre for Materials and Processes, Bremen, Germany.

Controlling the recrystallization is an important way to reach grain size refinement and outstanding strength and toughness on alloy metals. This study sets out the application and investigation of mathematical microstructure modeling of a newly designed bainitic steel for hot forging industrial applications. The macro-scale model was used to observe and predict the austenitic grain size behavior during the controlled forging of a gear. Arrhenius grain growth kinetic and recrystallization model for a new class of bainitic steel was established for the given strain rate ranges and temperatures. This model was calibrated through microscopic analysis and used to simulate the unpublished constants of low alloyed bainitic forging steel DIN 18MnCrSiMo6-4 microstructure module using DEFORM® commercial finite element code. The increased temperature due to the adiabatic effect was investigated by numerical analysis, demonstrating its influence on grain coarsening. Local tensile test and Charpy-V notch were compared at different industrial hot forging temperatures and local plastic strain. Changes in yield strength and ductility have demonstrated the grain size influence on the processing parameters. The employed numerical model was an efficient tool to predict and present an alternative path to develop robust industrial forging using semi-empirical models.

Keywords: *Hot Forging, Grain Size, JMAK, Mechanical Properties, Bainitic Steel.*

1. Introduction

Engineers and scientists have transformed how low alloyed carbon steels are designed and processed in the last decades. The relationship between tailored metals processing, microstructure, and mechanical properties remains challenging, especially when more energy-efficient and environmentally friendly products are on the global manufacturing agenda. Advanced bainitic steels have stood out in the last decades[1-4] due to the excellent combinations of mechanical properties such as yield strength and toughness caused by their microconstituents. One way to obtain such mechanical properties is prior austenitic grain size modification. It is known that coalescence of the bainite laths is avoided by grain refinement, increasing the volume fraction and stability of retained austenite in isothermal heat treatment[5]. Although it is an excellent method for this diffusional transformation, its mechanical performance is achieved at the cost of high energy consumption, making it less attractive in hot forged parts manufacturing chains.

As an alternative, the thermomechanical process in continuous cooling bainitic steels can lead to energy savings and tailored mechanical performance by controlling forging and cooling conditions, replacing long isothermal treatments such as quenching and tempering (Q&T)[2,4]. Therefore, understanding how these steels perform in hot forging applications is undoubtedly necessary to achieve excellent

mechanical properties. Efforts in understanding the bainitic transformation after the lower plastic strain was reported by[6] using in situ XRD experiments coupled with a dilatometer. Microstructure transformations in continuous cooling were accelerated after compression, and simultaneously, the granular bainite and retained austenite were refined. Another work[7] showed the effect of the plastic strain of metastable austenite on resulting bainite morphology by physical simulation. It has presented the doorway for the forging application using the DIN 18MnCrSiMo6-4 steel in different thermomechanical routes.

Silveira and co-workers[8] found that, besides the forging having a significant impact on the bainite morphology, at 1200 °C, a predominantly bainitic microstructure was formed from the coarse austenitic grains. They also summarized that plastic deformation at high temperatures inhibits the formation of pro-eutectoid ferrite, thus favoring the austenite transformation into bainite[7,8]. When the temperature was reduced to 1100 °C or 1000 °C, in addition to displaying more refined grains, there was an increase in the amount of polygonal ferrite and a reduction in retained austenite fraction. In summary, the austenitic grain significantly impacts the final microstructure of DIN 18MnCrSiMo6-4 steel.

In this way, and as acquired in an early work[9], the modeling of the flow curves of this material, as well as the (JMAK) "Johnson-Mehl-Avrami-Kolmogorov" parameters[10], are necessary for assessing its microstructural evolution such as in recrystallization kinetics. Thus, enabling the application

*e-mail: thiago.ivaniski@ufrgs.br

of "semi-empirical" numerical models, based on methods previously proposed by[11-17], which can simulate the complexity of the hot forging process and the grain size evolution.

Although the new methodology[11,13] is excellent for predicting grain size evolution and flow curves through the JMAK equation, it has not yet been applied in industrial hot forging in high strain rate presses (above 50 s^{-1}) in this bainitic steel. Also, the kinetics of austenitic grain growth industrial closed die hot forging after load release has not been discussed using a finite element FEM method approach. A higher strain rates increase dislocation density and stored energy during the plastic deformation, affecting recrystallization kinetics and possibly the grain growth[10]. In closed die forging, such behavior is expected. Therefore, in the present research, the suitability of these proposed methods was addressed in industrial hot forging conditions in a high strain rate press.

This work aimed at validating a macroscale model of the grain size evolution using numerical simulation for a new continuously cooled bainitic steel DIN 18MnCrSiMo6-4 hot forged. Some aspects regarding recrystallization during forging were addressed and what effects the process caused on grain growth. The synergetic effect between closed die forging parameters in response to austenitic grain size at the end of the process has been verified. Finally, it has compared two temperature levels on the mechanical properties.

2. Material and Methods

2.1. Grain growth kinetic of annealing test

All experiments were performed with the steel DIN 18MnCrSiMo6-4, classified as a low-carbon carbide-free bainitic steel grade. The chemical composition is given in Table 1.

The evolution of the austenitic grain size of this steel was studied by[8], considering the same sample mass of 515.47 g in a cylindrical geometry under isothermal conditions. The authors heated the samples at temperatures of 1000 °C, 1100 °C, and 1200 °C. It was found that the abnormal grain growth occurred at 1200 °C, which was attributed to the dissolution of precipitates formed by microalloying elements such as *Ti, N,* and *Al* in this steel. The reported results significantly explain the grain growth equation values, where the methodology is shown below to be discussed in the results section. Figure 1 shows the as received prior austenitic grain size PAGS and the microstructure of the steel revealed as the same methodology written in section 2.3.

The constitutive Arrhenius equation described grain growth kinetics[13]. In addition, the activation energy for this bainitic steel was determined according to Equation 1 implemented in DEFORM® V. 11.0 subroutine.

$$d = d_0^m + a_9 t \, exp\left(-\frac{Q_{gg}}{RT}\right)^{1/m} \tag{1}$$

The initial and final grain sizes are given by d_0 and d, while Q_{gg} describes the activation energy necessary for grain growth. The inverse of the time *t* exponent for grain growth is given by m, and a_9 is a constant that depends on the chemical composition of the steel[18]. The R-value is the universal gas constant (8.314 J/mol.K), and T the absolute temperature in Kelvin (K). By applying natural logarithm to both sides of Equation 1, we can determine m (Equation 2) and Q_9 (Equation 3) values, and it can be expressed as[13]:

Table 1. Chemical composition for steel 18MnCrSiMo6-4, mass percentage.

Element	C	Si	Mn	Ni	Cr	Cu	Mo	Al	Ti	N	Fe
Ma. %	0.18	1.19	1.42	0.063	1.17	0.10	0.27	0.005	0.004	0.01	Bal.
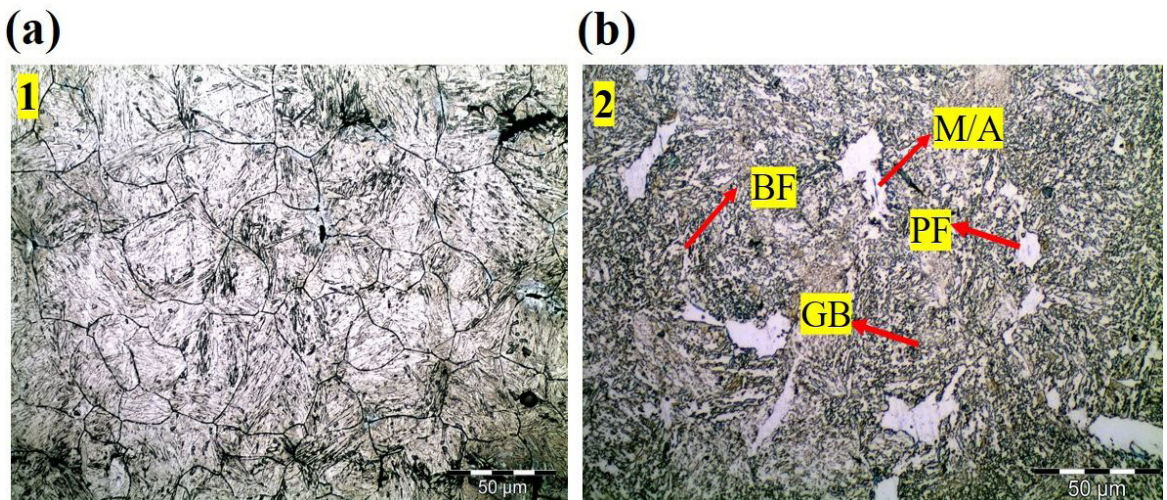
Figure 1. (a) 1 PAGS as received 23,5 μm, (b) 2 Initial Microstructure BF – Bainitic Ferrite, GB – Granular Bainite, PF – Polygonal Ferrite, A – Retained Austenite, M – Martensite.

Numerical and Experimental Study of an Industrial Case for Grain Size Evolution in Bainitic Steel in Controlled Hot Forging and its Influence on Mechanical Performance

3

$$\frac{1}{m} = \left| \frac{\partial lnd}{\partial \left(\frac{1}{t} \right)} \right|_T \tag{2}$$

$$Q_9 = -mR \left(\frac{\partial lnd}{\partial lnT} \right)_t \tag{3}$$

In this case, it is essential to emphasize that the equation describing growth does not consider prior plastic deformation. Moreover, the grain size distribution was assumed to be homogeneous since the grain size measurements were the same in distinct parts of the cylindrical rod obtained.

2.2. Flow curves and microstructure analysis

Hot isothermal compression tests for flow curves determination were conducted in a DIL 805A/T dilatometer. Cylindrical samples with 10 mm x 5 mm were heated at a rate of 10 °C/s and held for five (5) minutes for homogenization before compression. Strain rates of 0.1 s⁻¹, 0.5 s⁻¹, 1 s⁻¹, and 5 s⁻¹ and temperatures of 850 °C, 950 °C, 1050 °C, and 1150 °C with a fixed true plastic strain of 0.69 were set up for testing.

2.3. Metallography analysis

After isothermal compression and quenching, the austenitic grain size samples were prepared and analyzed by optical microscopy according to DIN EN ISO 643 and ISO 14250 using the line-intercept method. A saturated picric acid solution revealed the grain boundary (AGB) with 42 mL of wetting agent, 58 mL of distilled water, and 2.3 g of picric acid. Wetted cotton was swabbed into the steel surface for 5 min to reveal the (AGB). The overall microstructure was etched by immersion in a Nital 2% solution for 10 s.

Electron backscatter diffraction (EBSD) was performed using a Philips XL 30 to determine the distribution of the crystallographic units. The instrument operated at 25 keV, with a working distance of 8.4 mm, a sample tilt angle of 75 degrees, and a step size of 0.1 μm. The data were processed in Orientation Imaging Microscopy for two quenched samples in temperatures of 950 °C and 1150 °C at $\dot{\varepsilon} = 0.1$ s⁻¹ of plastic strain rate.

2.4. Recrystallization model

The modeled flow curves obtained by compression tests and the JMAK recrystallization coefficients were implemented in DEFORM® finite element code V11.0. Figure 2 shows the flowchart used for the acquisition of the coefficients.

The Zener-Hollomon parameter Z was calculated using Equation 4, and the overall equation that depends on it is shown in Equation 5.

Where Z is:

$$Z = \dot{\varepsilon}.exp\left(\frac{Q}{RT} \right) \tag{4}$$

In Equation 5, n, α, and A are the material-dependent constants, determined by experimental flow curve results, and Q is the activation energy in (J/mol.K) for the onset of dynamic recrystallization.
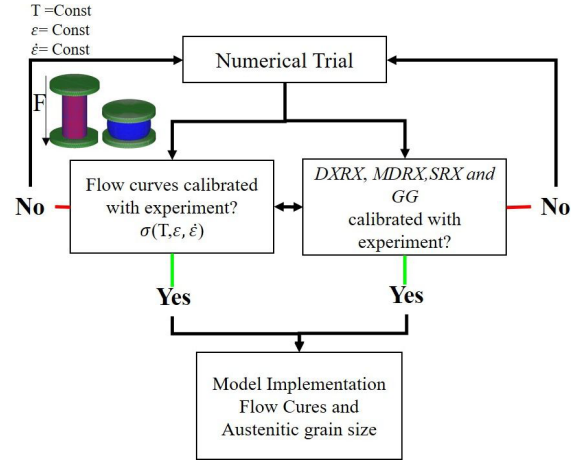

Figure 2. Flowchart of modeling interaction to calibrate the experiment.

The parameters determined from flow stress curves for the DIN 18MnCrSiMo6-4 steel were $\alpha = 0.009833$ MPa⁻¹, $n = 5.3$, $A(T. \bar{\dot{\varepsilon}}) = 7.6 \times 10^{11}$ and $Q_{Total} = 276684$ J/mol.K[9]. The peak stress σ_p was defined by deriving the stress and strain from the flow curves ($\theta = \frac{\partial \sigma}{\partial \varepsilon}$).

$$\dot{\varepsilon} = A \left[\sinh\left(\alpha \sigma_p \right) \right]^n exp\left(\frac{Q}{RT} \right) \tag{5}$$

The modeled flow stress in the subroutine of the finite element code is shown in Equation 6, where the work hardening σ_{WH} represents the stress caused by the increase in dislocation motion of the material up to σ_p.

$$\sigma_{WH} = \sqrt{\left(\sigma^2_{sat} - \left(\sigma^2_{sat} - \sigma_0^2 \right) exp\left(-r\varepsilon \right) \right)} \tag{6}$$

Where σ_{WH} is derived from the saturation stress σ_{sat}, which is the first stage in which flow stress increases. Where r is the dynamic recovery coefficient that decreases as the strain rate increases in DIN 18MnCrSiMo6-4 bainitic steel[9], this coefficient has an essential function in this work, as it improves the model accuracy at high strain rates in the hot forging process.

Since these coefficients are obtained by linear fitting from the experimental results already determined by[9], the stress model can be calculated via Equation 7. The σ_{ss} represents the stress at a steady-state when complete dynamic recrystallization X_{DRX} occurs.

$$\sigma_{mod} = \sigma_{WH} - \left[\sigma_{sat} - \sigma_{ss} \right] \cdot X_{DRX} \tag{7}$$

A more detailed description of these hyperbolic constitutive equations and how these results were obtained for this steel can be found in[9].

The mathematical model of the critical strain before reaching a steady-state is presented in the following equation (Equation 8) and has been proposed in several previous works[16,18,19] for C-Mn steels. When the critical strain (ε_c) is exceeded, as described in Equation 7, new grains nucleate and grow during the strain step only for $\bar{\varepsilon} > \varepsilon_c$.

$$\varepsilon_c = a_2 \cdot \varepsilon_p \tag{8}$$

In Equation 8 and Equation 9, $a_1, a_2, n_1, m_1,$ and   are the dependent material parameters and the peak strain, respectively, which is equal to the peak stress σ_p derived from the flow curves.

The activation energy Q_1 (J.mol^{-1}), gas constant R (J.mol^{-1}. K^{-1}), and the initial grain size d_0 depend on the effective strain rate $\dot{\bar{\varepsilon}}$, and the temperature T. Thereby, Equation 8, Equation 9, and Equation 10 describe the overall kinetics of dynamic recrystallization X_{DRX}.

$$\varepsilon_p = a_1 \cdot d_0^{n_1} \cdot \dot{\bar{\varepsilon}}^{m_1} \cdot exp\left(\frac{Q_1}{RT}\right) \tag{9}$$

$$X_{DRX} = 1 - exp^{\left(\beta_d\left(\frac{\varepsilon - \varepsilon_p \cdot a_{10}}{\bar{\varepsilon}_{0.5}}\right)^{k_d}\right)} \tag{10}$$

In Equation 10, the exponent (β_d) represents the Avrami coefficient which is sensitive to variations in temperature. The Avrami exponent (k_d) is determined by polymorphic changes, discontinuous precipitation, and interfacial growth control, among other factors[18,19]. The $\bar{\varepsilon}_{0.5}$ described in Equation 11 is the strain when 50% of the recrystallized fraction is reached, where $a_5, h_5, m_5,$ and n_5 are material parameters.

$$\bar{\varepsilon}_{0.5} = a_5 d_0^{h_5} \dot{\bar{\varepsilon}}^{m_5} \varepsilon^{n_5} exp\left(\frac{Q_5}{RT}\right) + C_5 \tag{11}$$

Finally, Equation 12 and Equation 13 provide the recrystallized grain size D_{DRX} after full X_{DRX} and the average grain size D_{AVG}, respectively.

$$D_{DRX} = a_8 d_0^{h_8} \dot{\bar{\varepsilon}}^{m_8} \varepsilon^{n_8} exp\left(\frac{Q_8}{RT}\right) \tag{12}$$

$$D_{AVG} = X_{DRX} D_{DRX} + (1 - X_{DRX}) d_0 \tag{13}$$

If, after the interruption of deformation, the cumulative strain during the industrial forging process is higher than the critical strain (ε_c) then metadynamic recrystallization occurs[18]. In M_{DRX}, new nuclei appear during forming, but grain growth occurs after the onset of plastic strain. Equation 14 and Equation 15 describe the kinetics:

$$X_{MDRX} = 1 - exp^{\left(\beta_m\left(\frac{t_{sec}}{t_{0.5}}\right)^{k_m}\right)} \tag{14}$$

$$t_{0.5} = a_4 \bar{\varepsilon}^{n_4} d_o^{h_4} \dot{\bar{\varepsilon}}^{m_4} exp\left(\frac{Q_4}{RT}\right) \tag{15}$$

Where $t_{0.5}$ is the time required for 50% metadynamic recrystallization, which is dependent on the effective strain $\bar{\varepsilon}^{n_4}$, initial grain size $d_o^{h_4}$ and strain rate $\dot{\bar{\varepsilon}}^{m_4}$ exponents. Equation 16 describes the grain size diameter for a complete metadynamic recrystallization after plastic strain:

$$D_{MDRX} = a_7 \bar{\varepsilon}^{h_7} d_0^{h_7} \dot{\bar{\varepsilon}}^{m_7} exp\left(\frac{Q_7}{RT}\right) \tag{16}$$

Static recrystallization, described in Equation 17, occurs when the cumulative strain is lower than the critical strain (ε_c). During this phenomenon, nuclei of recrystallized grains appear and grow after the forging step. The equation is given by:

$$X_{SRX} = 1 - exp\left(\beta_s\left(\frac{t}{t_{0.5}}\right)^{k_s}\right) \tag{17}$$

Where $t_{0.5}$, Equation 18 is:

$$t_{0.5} = a_3 \bar{\varepsilon}^{n_3} d_o^{h_3} \dot{\bar{\varepsilon}}^{m_3} exp\left(\frac{Q_3}{RT}\right) \tag{18}$$

Grain growth for a full S_{RX} is given in Equation 19:

$$D_s = a_6 \bar{\varepsilon}^{n_6} d_0^{h_6} \dot{\bar{\varepsilon}}^{m_6} exp\left(\frac{Q_6}{RT}\right) + C \tag{19}$$

After full dynamic, static and metadynamic recrystallization, equiaxed grains may coarsen due to grain growth, as described in Equation 20, which is considered temperature-dependent.

$$d_f^{m(T)} = d_{0drx}^{m(T)} + a_9 exp\left(-\frac{Q_9}{RT}\right).t \tag{20}$$

Here, d_0 is the full-recrystallized grain size, t is the time after complete recrystallization, Q_9 is the apparent activation energy, and m and a_9 are the material and process-dependent constants.

2.5. Forging trial and numerical modeling

The industrial closed die forging tests were performed using a friction press with an energy of 240 kJ. Table 2 shows the forging conditions and targets used in this work. A cylindrical billet was forged at two different temperature conditions. The thermomechanical route and a forged specimen are shown schematically in Figure 3.

After forging, two dwell times, which represent the interval before quenching, were estimated with the aid of recorded videos. The first dwell time represents the interval where the lower and upper dies touch, 2 seconds. The second dwell time represents the interval in which the upper die was lifted, allowing the workpiece to be manipulated/moved. The workpiece was then quenched with moderate agitation at a water temperature of 23 °C.

After the first methodology was used for forging and quenching, other samples were forged and cooled to room temperature (25 °C) in calm air. Three representative sample regions were analyzed to determine the average grain size after hot forging. Prior austenitic grain size (PAGS) after quenching with water was revealed using a 3% picric acid solution and quantified by optical microscopy at 500x magnification. The circular intercept method was used for grain size determination of the hot-forged samples according to the ASTM E112 standard[20].

Numerical and Experimental Study of an Industrial Case for Grain Size Evolution in Bainitic Steel in
Controlled Hot Forging and its Influence on Mechanical Performance

5

The evolution of the grain size of steels by induction coil heating at 1030 °C and 1130 °C after 300 seconds was studied in annealing tests, which gave values of 26 μm for 1030 °C and 54 μm for 1130 °C. After removing the samples from the induction furnace, the surface temperature was measured using a Fluke®, Ti - 400 thermal camera. The forging temperatures in this work were chosen to be 1030 °C and 1130 °C based on the results of[8] to avoid abnormal austenitic grain growth.

The coupled simulation of heat transfer and microstructure evolution was performed using a rigid-viscoelastic code in DEFORM® V.11.0. The multi-operation code was used to represent the industrial conditions in the numerical simulation. Figure 4 shows the proposed forging model corresponding to the industrial conditions and the tracked points representing the average grain size of twelve points in the measured regions (R1, R2, and R3).

Hexahedral elements were used to discretize the components using a coupled thermomechanical process. Elasto-plastic bodies were considered in the upper, lower, and knock-off dies, with 250 °C as the initial temperature in the forming dies. Since high plastic strains lead to severe mesh distortion, the automatic remeshing technique was used. This method solves problems related to the inability to model geometry and state variables[19].

The boundary conditions of the process are listed in Table 3, according to the industrial environment and the steel properties. The thermal conductivity and heat capacity were taken from Castro et al.[21] inverse heat transfer analysis for this steel. The friction factor μ was set at 0.3, corresponding to the use of graphite and water in the closed die hot forging condition[14].

2.6. Strength and toughness analysis

This study performed tensile testing of the miniature specimen to determine strength in specific forged areas, as shown in Figure 5. A hydraulic testing machine MTS 810 250 kN with a laser strain gage, was used to perform the tests. For each analyzed region, seven (7) samples were prepared for testing to achieve good repeatability of the experiments. The samples were produced by wire EDM, as suggested by[22], using the standards DIN EN 2002:2006, DIN EN ISO 6892-:2009-12, and DIN 50100. Four specimens were taken from two forged test pieces for each temperature proposed in this study to determine the bar impact energy by the Charpy notched bar impact test. The specimens were tested at a room temperature of 23.5 °C in a standard atmosphere. The specimens were processed following ASTM E2298[23].

Table 2. Processing conditions in the industrial forging experiments.

Forging type	Initial geometry (mm)	Temperature (°C)/ Induction coil power (kW)	Forming speed (mm/s)	Cooling program	Cooling rate (°C/s)	Revealing type
Closed die	54 x 38	1030, 32.9	1645	Water quenching	~ 45	Austenite grain boundaries
		1130, 40.6		Continuous cooling	~ 0.7, 0.65	bainite, ferrite, martensite

Table 3. Thermal properties in the numerical model.

Item	Value
Density (g/cm³)	7.83
Heat transfer with pressure considering scale field (N/sec/mm/°C)	11
Air convection coefficient (N/sec/mm/°C)	0.01
Quenching convection coefficient (N/sec/mm/°C)	11
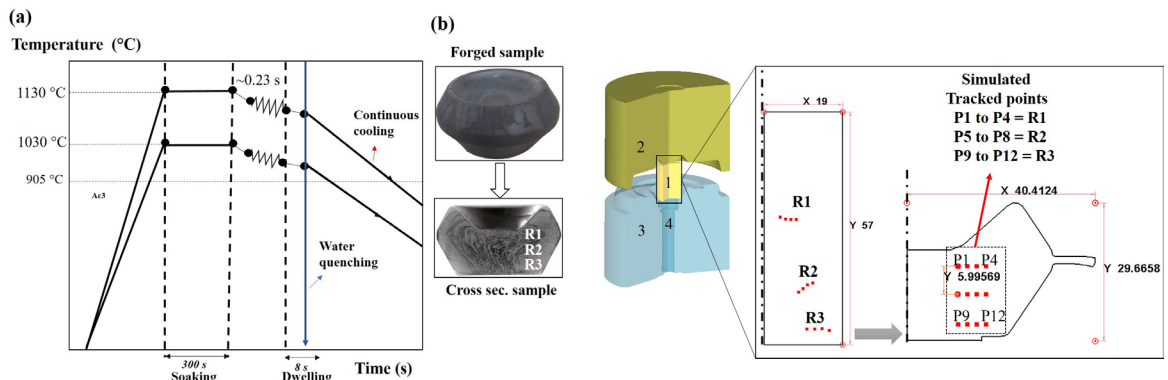
Figure 3. (a) Thermomechanical routes on industrial environment steps, (b) Experiment forged samples indicating the regions of metallography analysis.

Figure 4. The axisymmetric model implemented in DEFORM for gear forging and a cross-section of the simulated forging profile of the preform showing the analyzed areas. 1 - Billet, 2 - Upper die, 3- Lower die, 4 - Knock-off.
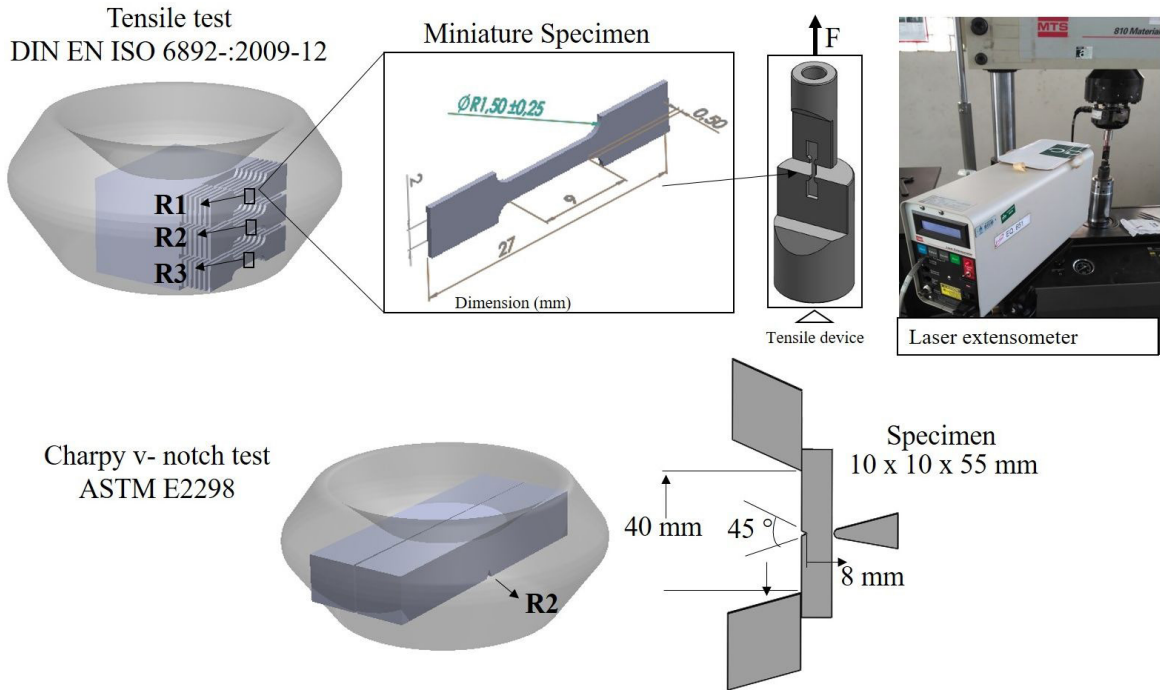
Figure 5. Representative and machined zone of collected samples for the miniature tensile test specimen and Charpy V-notch.

3. Results and Discussion

3.1. Grain growth model of annealing

Figure 6a and 6b show a parallel trend in grain growth with increasing time and temperature. Linear regression was used to estimate the mean values of the coefficients m, a_9, and Q_9 given in Equation 21.

From these data fitting, Figure 6c shows the results of the isothermal numerical simulation of austenitic grain growth compared to the experiments performed by[8]. In the current study, it was necessary to consider a homogeneous grain size distribution to find a reasonable agreement between the experiment and predicted results.

$$d = d_0^{5,25} + 4.56 \cdot 10^{16} t \, exp\left(-\frac{299500}{RT}\right)^{0.1904} \quad (21)$$

Figure 6c also shows that grain growth exhibits exponential behavior, with final size strongly affected by temperature after a short time. At a specific annealing time, say 1200 seconds, a variation in grain size deviates from the exponential trend. It is possible that at this point, a change in activation energy occurs, possibly changing the exponent (m) in Equation 1 of grain growth. In particular, this is caused by dissociating precipitates that reduce grain growth's boundary motion or coalescence due to Zenner pinning[8].

It is well known that carbon diffuses rapidly because of its interstitial characteristics, facilitating dissolution in the austenitic matrix. Therefore, it requires less self-diffusion activation energy. The opposite is true in the presence of substitutional elements such as *Mn* and *Ti*, which require higher self-diffusion activation energy[24].

The abrupt increase in austenite grain size at 1200 °C is the result of the dissolution of carbides formed by microalloying elements in this steel. These elements are responsible for forming precipitates such as manganese sulfides MnS and TiC, which causes pinning effects to be a barrier to grain growth[8]. Molybdenum carbides (*MoC*) may have formed since a small amount (~0.27% *Mo*) is present, affecting grain growth stabilization.
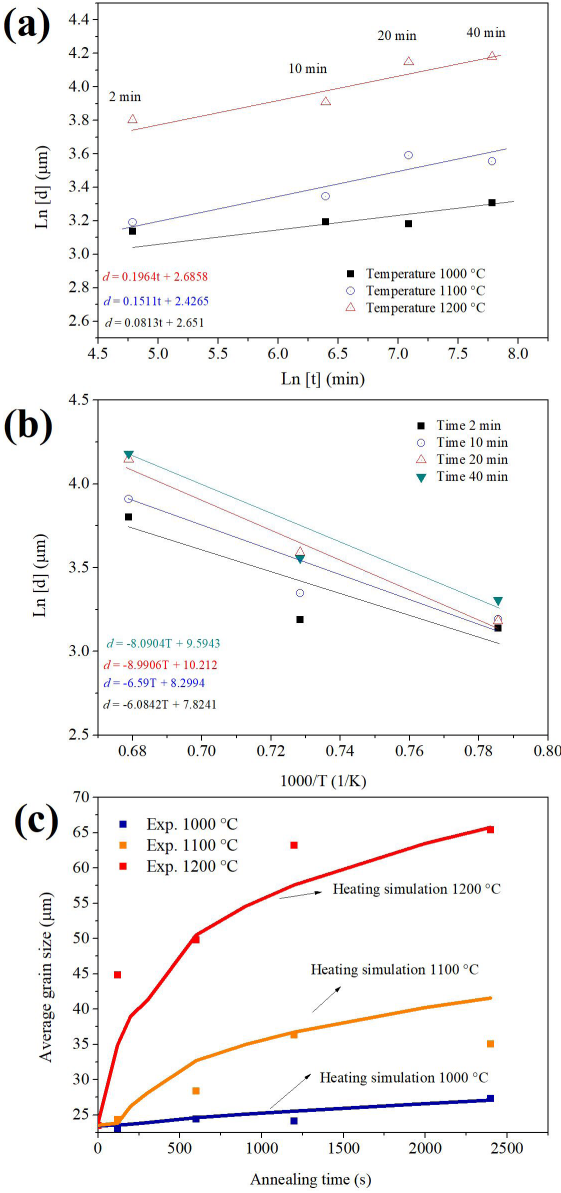
The theoretical implications may suggest that the total grain boundary area, in this case, is higher than the 1200 °C austenitization condition. Therefore, the system's total energy may be higher[24]. In other words, it can be assumed that the activation energy increased.

The value of the activation energy of 18MnCrSiMo6-4 is (299 kJ/mol.K), which is slightly higher than the results calculated by[13] (230.992 kJ/mol.K), which was determined for a steel grade with a higher carbon content of 0.3% C and lower amount of manganese 0.81% Mn. However, after the annealing test, the obtained grain size in this work is smaller than the steel studied by[13] (about 7.8 times lower).

3.2. Model validation

This work's industrial application model has been based on validating the numerical model of grain growth after the recrystallization kinetics from the compression test. The interactive mode presented in Figure 2 determines the coupling of the flow curve and grain size model throughout the experimental results. Table 4 displays the overall constants calibrated for the microstructure modeling.

The accuracy of the results of the FEM model can be seen in the flow stress shown in (Figure 7a), which shows what would be the flow curves at high strain and strain rate levels

Numerical and Experimental Study of an Industrial Case for Grain Size Evolution in Bainitic Steel in
Controlled Hot Forging and its Influence on Mechanical Performance

7

(a)

$d = 0.1964t + 2.6858$
$d = 0.1511t + 2.4265$
$d = 0.0813t + 2.651$

(b)

$d = -8.0904T + 9.5943$
$d = -8.9906T + 10.212$
$d = -6.59T + 8.2994$
$d = -6.0842T + 7.8241$

(c)

Figure 6. Modeled Annealing curves for 18MnCrSiMo6-4 steel;
(a) Natural logarithm of grain size and time, (b) Grain size and
inverse of temperature, (c) Comparison between experiment[8] and
simulation grain growth evolution.

$(100\ s^{-1})$. These curves were converted into time (s) format
using the ratio between the strain and strain rate (s^{-1})[9,10], as
shown in Equation 22. In (Figure 7b), the predicted values of
recrystallization fraction in different strain rates are shown.

$$t = \left(\frac{\varepsilon - \varepsilon_c}{\dot{\varepsilon}}\right) \quad (22)$$

With the increase of strain rate at constant T (1150 °C),
the X_{DRX} time decreased[18]. As reported by[10,25], a high strain
rate increases the migration rate of dislocations and grain
boundaries, therefore, accelerating the X_{DRX} process after
the ε_c is reached[25].

Figure 7c and 7d show the predicted results of the
experimental punch load of the numerical model during
the compression test and FEM recrystallization results,
respectively.

A good approximation of the computational simulation
results with the force and displacement experiments has
been shown, using the model proposed by[9] for a continuous
cooling bainitic steel. A slight variation of the experimental
forces compared to the simulation can be seen at the
temperature and strain rate of 950 °C and 5 s^{-1}, respectively.
It is assumed that this condition is more prone to adiabatic
heating variation for the calculated model when compared
to the phenomena occurring during the experiment. The
chemical interactions and the activation energy vary with
the degree of plastic strain and strain rate. Therefore, this
can sensitively vary the force and displacement results.
Moreover, friction was kept constant during the computer
simulation, not depicting the natural behavior during the
hot forging process. A dynamic friction coefficient could
be preferred to solve this issue.

Figure 8 shows the cross-section view of the
experimentally measured and numerically calculated
fully recrystallized austenitic microstructure after
being compressed at 950 °C (Figure 8a) and 1150 °C
(Figure 8b), respectively. Three points on the specimens
were measured and compared to the simulation. What
stands out in this figure is that small nucleate recrystallized
grains can be observed at different temperatures, with
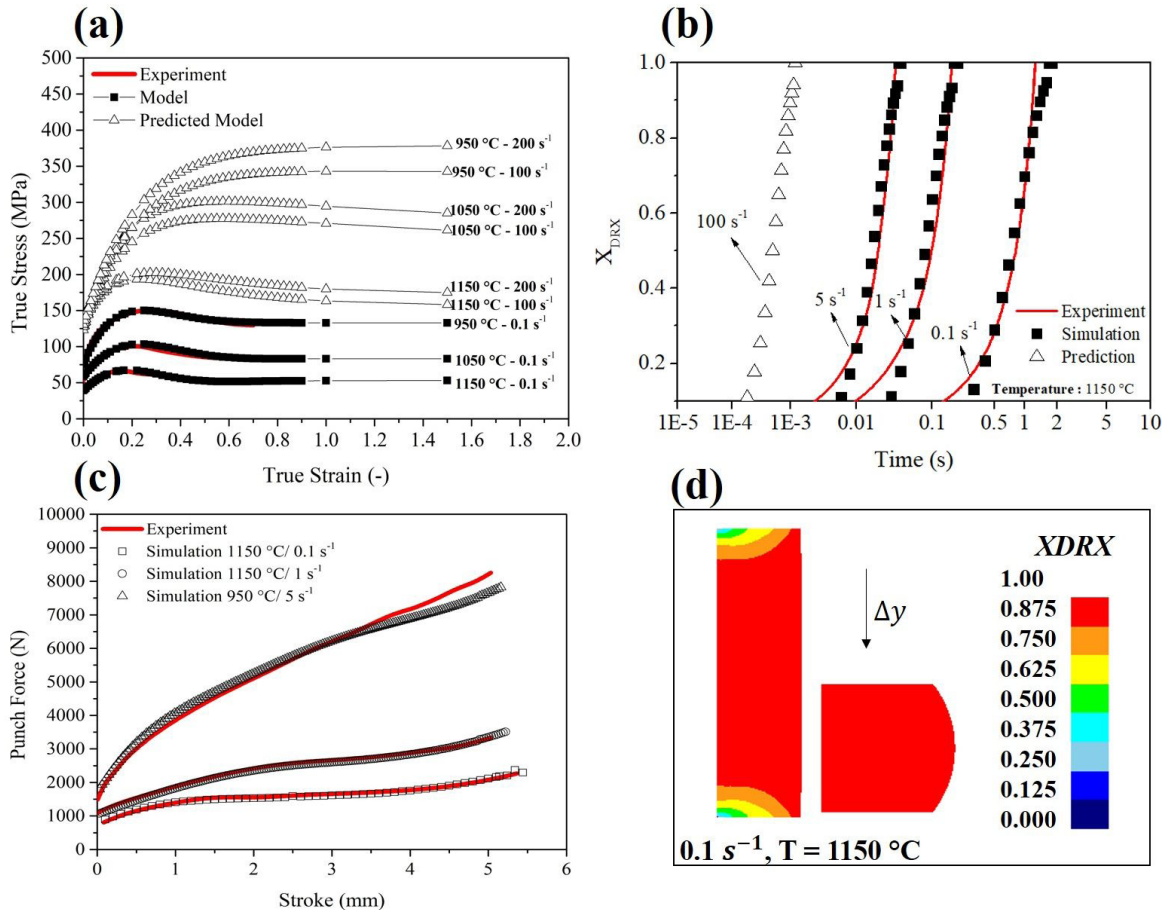grains being more refined at 950 °C.

Figure 9 illustrates the experimental and simulated
austenitic grain size variation at different temperatures and
strain rates. The most interesting aspect of this graph is that
the temperature influenced the austenitic grain refinement
and the strain rate. The values show that increasing the
strain rate by 10 times at 1150 °C caused a higher variation
in grain size when compared to 950 °C. The variation was
40.74% at a constant temperature of 1150 °C. A percentage
variation of 82% in the grain size refinement was obtained
from 1150 °C to 950 °C. However, at 950 °C, the strain
rate did not influence the grain refinement considerably.
That behavior could be related to a decrease in driving
force where the temperature dominates the recrystallization
mechanism activation[9,15].

The EBSD map in Figure 10 shows these results in
the crystallographic unit sizes (UC) of quenched samples,
and Figure 11 shows a histogram of the UC. Smaller
crystallographic units were seen in the sample compressed
at 950 °C (Figure 10a) than in the samples at 1150 °C
(Figure 10b). At 950 °C, less UC size distribution was
observed, as shown in (Figure 11a) in comparison to the
higher forming temperatures (Figure 11b), which showed
a more extensive UC distribution. Also, a morphological
variation, where more granular packages were seen at lower
temperatures whereas, at higher temperatures, large packages
with laths were observed.

The smaller austenitic grain sizes were assumed to be
responsible for the smaller crystallographic UC, which
contribute to the increase in high-angle grain boundaries
(HAGB), which, according to the literature[26,27], improves
the material's toughness and strength.

Table 4. Constants used in DEFORM® after calibration of the experiment for microstructural modeling of DIN 18MnCrSiMo6-4 steel.

Constants of Microstructure Evolution							
Critical Strain ε_c	Values	X_{DRX} and D_{DRX}	Values	M_{DRX} and D_{MRX}	Values	S_{RX} and D_{SRX}	Values
a_1	0.00479	β_d	-0.597	β_m	0.69417	β_S	-0.6931
a_2	0.54	k_d	1.798	k_m		k_s	1
n_1	0	a_5	0.1129	a_4	2.13E-6	a_3	2.5E-19
m_1	0.1238	h_5	0.32	h_4	0	h_3	0
Q_1	44500	n_5	0	n_4	0	n_3	-4.0
		m_5	0.03	m_4	-0.62	m_3	2.0
		Q_5	3450	Q_4	133000	Q_3	270000
		c_5	0	a_7	1804.6	a_6	0.5
		a_{10}	0	h_7	0.63	h_6	0.67
		a_8	8103	n_7	-0.25	n_6	-1
		h_8	0	m_7	-0.12	m_6	0
		n_8	0	C_7	0	c_6	0
		m_8	-0.16	Q_7	-73778	Q_6	0
		c_8	0				
		Q_8	-74880				

Figure 7. (a) Modeled flow curves and predicted for high strain rates on temperature dependence[9], (b) X_{DRX} kinetics on strain rate dependence, modeled and predicted, (c) Comparison between experiment and prediction of a load of a compression test, (d) FEM recrystallization results.
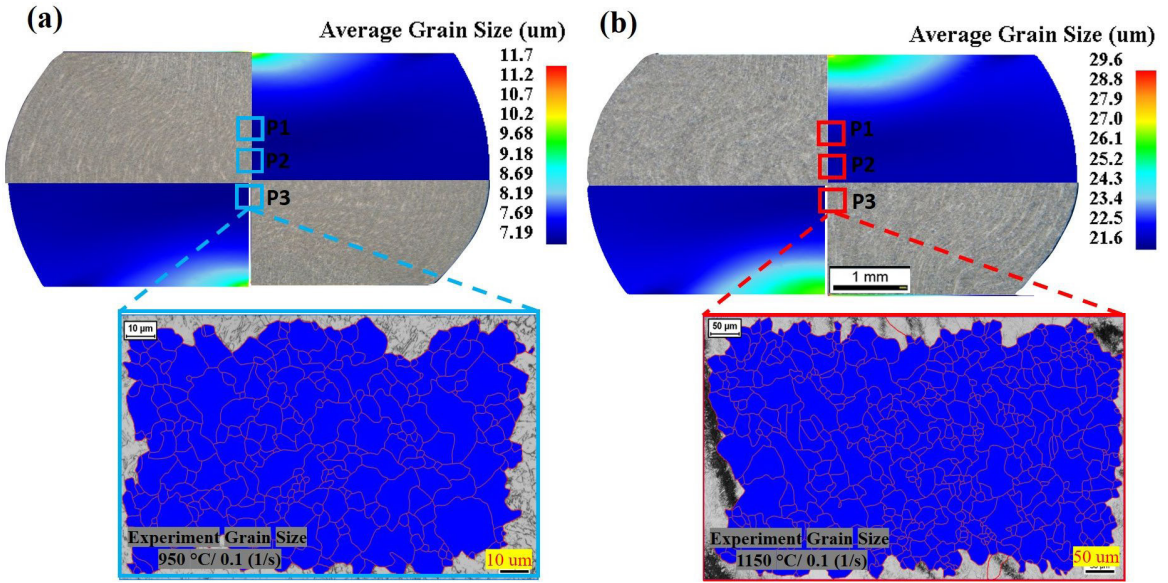
Numerical and Experimental Study of an Industrial Case for Grain Size Evolution in Bainitic Steel in
Controlled Hot Forging and its Influence on Mechanical Performance

9

Figure 8. Simulation of austenitic grain size in isothermal compression test (a) 950 °C, 0.1 (1/s), (b) 1150 °C , 0.1 (1/s).
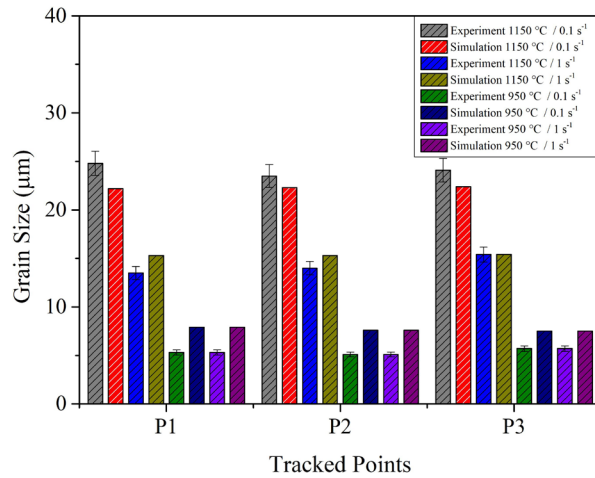

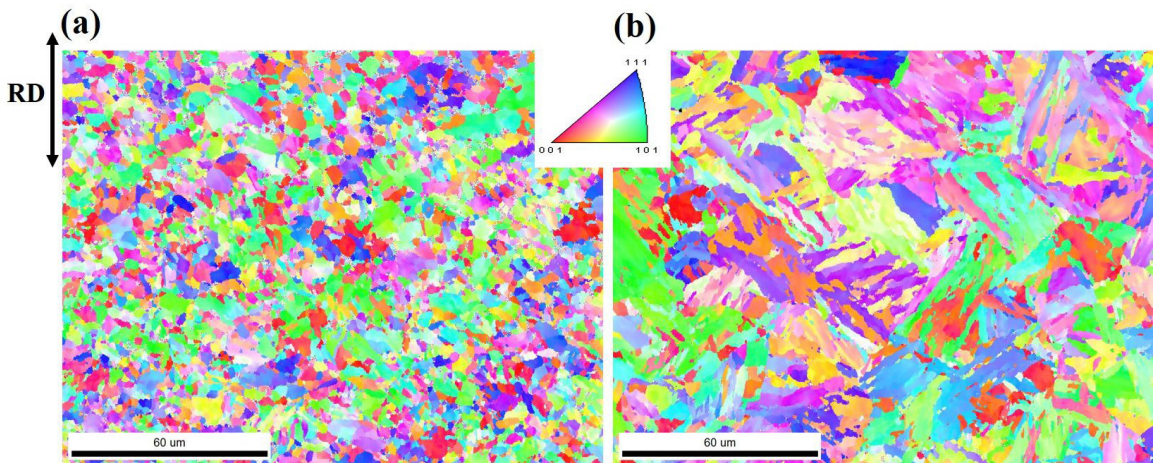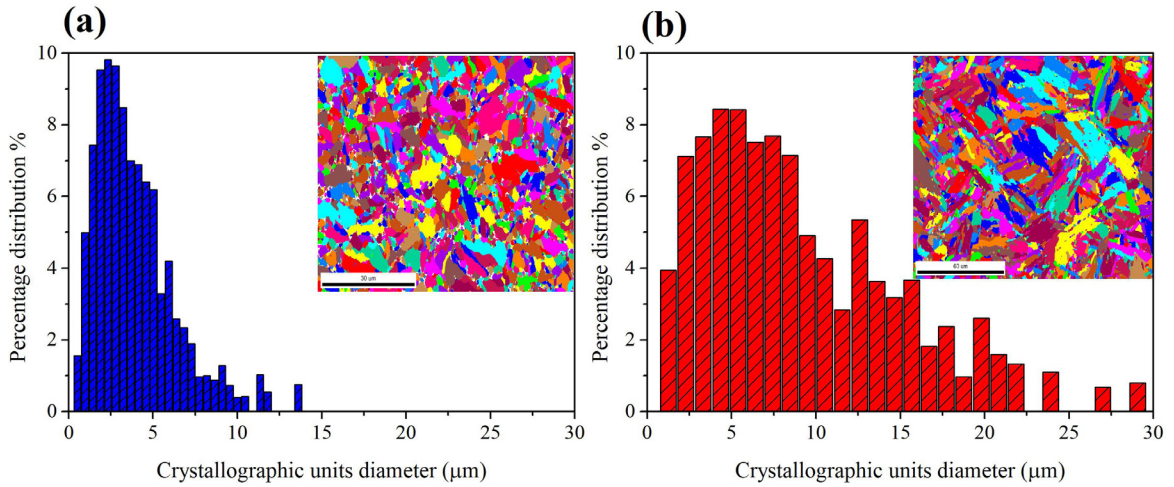**Figure 9.** The predicted austenitic grain size of hot compressed samples ε = 0.69.

Figure 10. EBSD map showing the temperature dependence in different sizes of crystallographic units. (a) P3 - T = 950 °C / $\dot{\varepsilon}$ = 0.1 s^{-1},
(b)P3 - T = 1150 °C / $\dot{\varepsilon}$ = 0.1 s^{-1}.

(a)

(b)

Figure 11. Histogram of measured crystallographic units grain sizes, (a) T = 950 °C / $\dot{\varepsilon}$ = 0.1 s^{-1}, (b) T = 1150 °C / $\dot{\varepsilon}$ = 0.1 s^{-1}.

3.3. Industrial application

3.3.1. Hot forging simulation results

A point-tracked section of DIN 18MnCrSiMo6-4 helical gear was analyzed in the simulation results. The average temperature of the tracked points displayed in (Figure 4), representing each analyzed region (R1, R2, and R3) in the simulation, is shown in Figure 12.

The temperature rises due to the energy dissipation in the form of heat (adiabatic heating) caused by strain rate and plastic strain, showed in (Figure 13a) and (Figure 13b). The simulation results show that the energy dissipation is higher during forging with the initial temperature of 1030 °C than 1130 °C due to mechanical energy available to be converted into heat being higher in lower temperatures. There was an increase of 50 °C from the temperature of 1030 °C and 30 °C at the temperature of 1130 °C.

The conduction between the workpiece and dies provokes a decrease in temperature on both surfaces, which is more pronounced for the lower die, as shown after a dwelling of 2.023 seconds. Moreover, the heat flux from region R3 in direction to region R2 and R2 to R1 maintains R2's temperature constant for a longer time and, therefore, causes an increase in the austenitic grain size by grain coarsening. This behavior is shown in (Figure 12a) for forging at 1030 °C and (Figure 12b) for forging at 1130 °C.

Lower temperatures also increase the force required for the plastic flow and, therefore, the system's energy[19]. Even with the increase in energy dissipation in higher strain rates, forging at lower temperatures (1030 °C) does not exceed the value of 1100 °C-in this way, avoiding the excessive grain coarsening.

Although these behaviors are expected, it is only through FEM that it can accurately quantify the local distribution of strain throughout the billet, allowing evaluation of mechanical properties after the tensile and impact tests. The numerical simulation showed a significant difference between the effective strain rate fields in the R2 region and R3 caused by the upper die piercing in the billet, changing the plastic flow rate.

Even though the increase in strain rate should reduce the recrystallization fraction due to the increase in critical strain for X_{DRX}[16], we must take into account the adiabatic heating in high-speed closed die forging, which interacts in two ways: First, through the heterogeneous plastic strain, which was higher in R1 than in R2 and R3, and second, through the heterogeneous strain rate, which changes the parameter (Z) responsible for the magnitude of D_{DRX}. Thus, the simultaneous increase in plastic strain and strain rate in R1 resulted in a higher X_{DRX} fraction due to the temperature increase, which delayed the time of grain growth by increasing the dynamically recrystallized grains D_{DRX}.

Different mechanisms such as X_{DRX}, M_{DRX}, and S_{RX} can be qualitatively analyzed through FEM by the JMAK macro-scale model results. Figure 14 provides the results obtained from the numerical simulation of these phenomena, and, Figure 15 shows the grain size evolution. According to these results, when ($\bar{\varepsilon} > \varepsilon_c$), there is a predominance of X_{DRX} (Figure 14a), which is proportional to the plastic strain in each selected region.

Nonetheless, compared to the analyzed regions R1, R2 and R3, the strain rate may also be responsible for the lower X_{DRX} values found in R2 and R3. It is well known that strain rate affects the dynamic recrystallization kinetics due to the increase in dislocation density[16]. Higher strain rates may decrease the mobility of these dislocations in R2 and R3, which consequently reduces annihilation or rearrangement. In contrast, in the R1 region, which may increase mobility due to higher temperature, over 95% of complete recrystallization was achieved.

The regions that were submitted to minor plastic strain and lower than critical strain ε_c was recrystallized Metadynamically (M_{DRX}) and statically (S_{RX}), respectively, as shown in Figures 14b and 14c. An apparent phenomenon is that the M_{DRX} is slower than the *DRX*'s kinetics and is observed in R1. Therefore, the significant difference between each recrystallization phenomenon is that the final nucleated grain size may be larger than the X_{DRX} at the same deformation time as holding. The main reason for this phenomenon is the lack of dislocation multiplication during the M_{DRX} process[28].

Numerical and Experimental Study of an Industrial Case for Grain Size Evolution in Bainitic Steel in
Controlled Hot Forging and its Influence on Mechanical Performance

11

In the case of closed-die forging, such a mechanism could be compensated by the temperature rise caused by the stored energy due to the plastic strain, strain rate, and the heat dissipation itself. The higher forging temperature (1130 °C) and strain rate may provide more thermal energy for grain boundary migration[29]. In R2, the temperature was higher than in R1 after 8.23 s, as shown in Figure 12b, and

therefore more thermally activated for the grain growth mechanism (Figure 15b).

3.3.2. Grain growth simulation after hot forging

Based on the results in Figure 10 and the discussion in the previous section, we have considered the grain growth exponent m (Equation 20) as a variable, which depends on
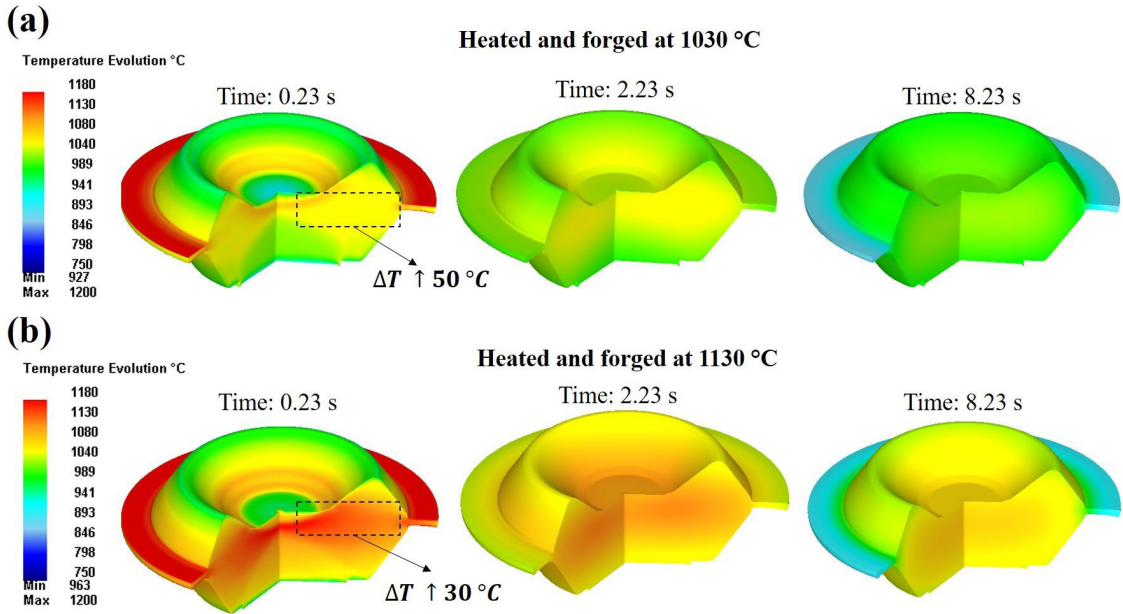

Figure 12. Temperature evolution of forging and cooling simulation in the forged preform; (a) Austenitization at 1030 °C; (b) Austenitization at 1130 °C.
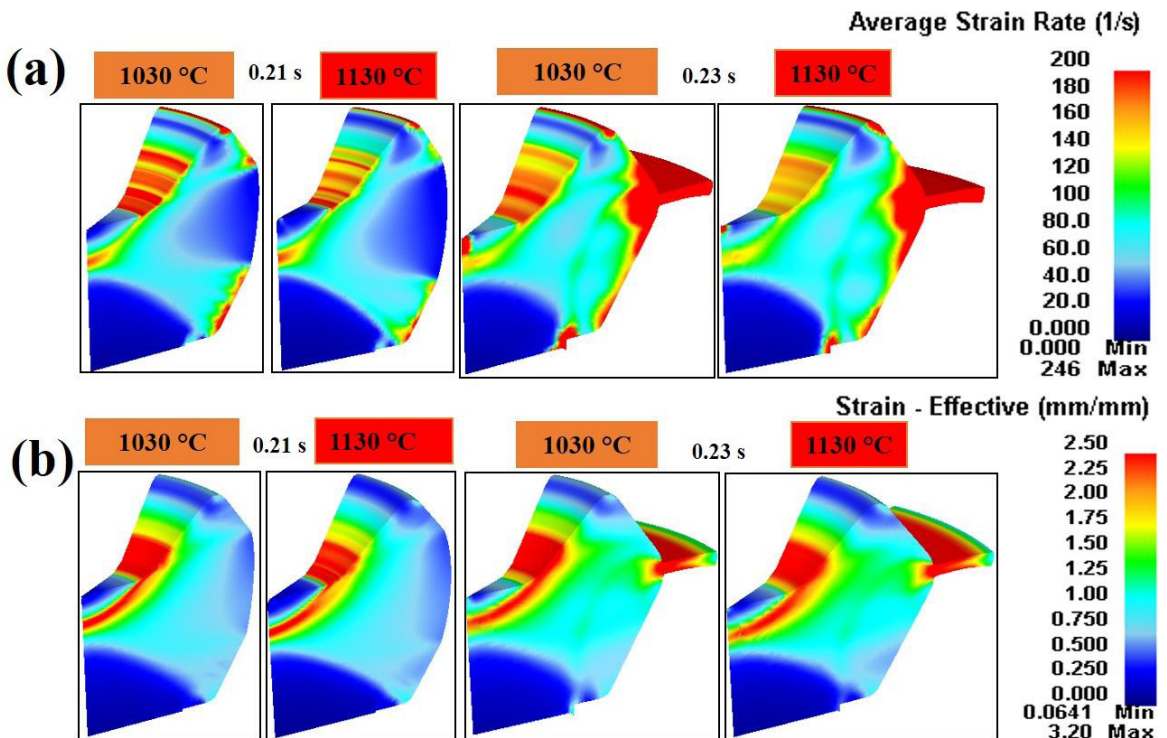

Figure 13. Simulated evolution of (a) average strain rate ($\dot{\varepsilon}$) and (b) effective strain ($\bar{\varepsilon}$) on the industrial preform forged gear.
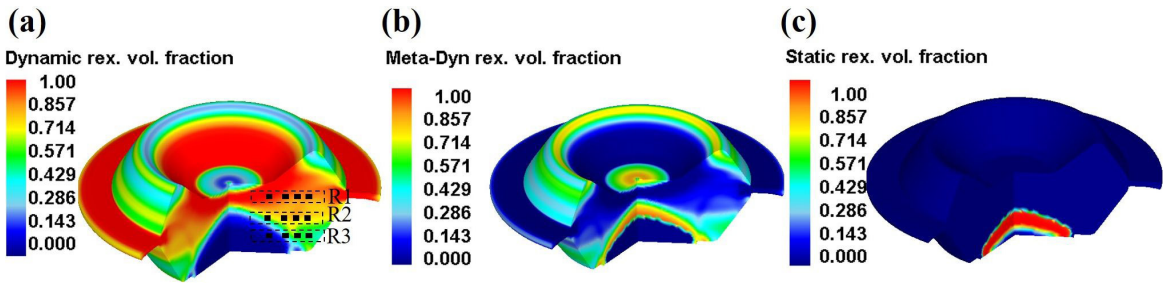
Figure 14. Recrystallization kinetics of the modeled preform hot forged; (a) X_{DRX}; (b) M_{DRX}; (c) S_{RX}.
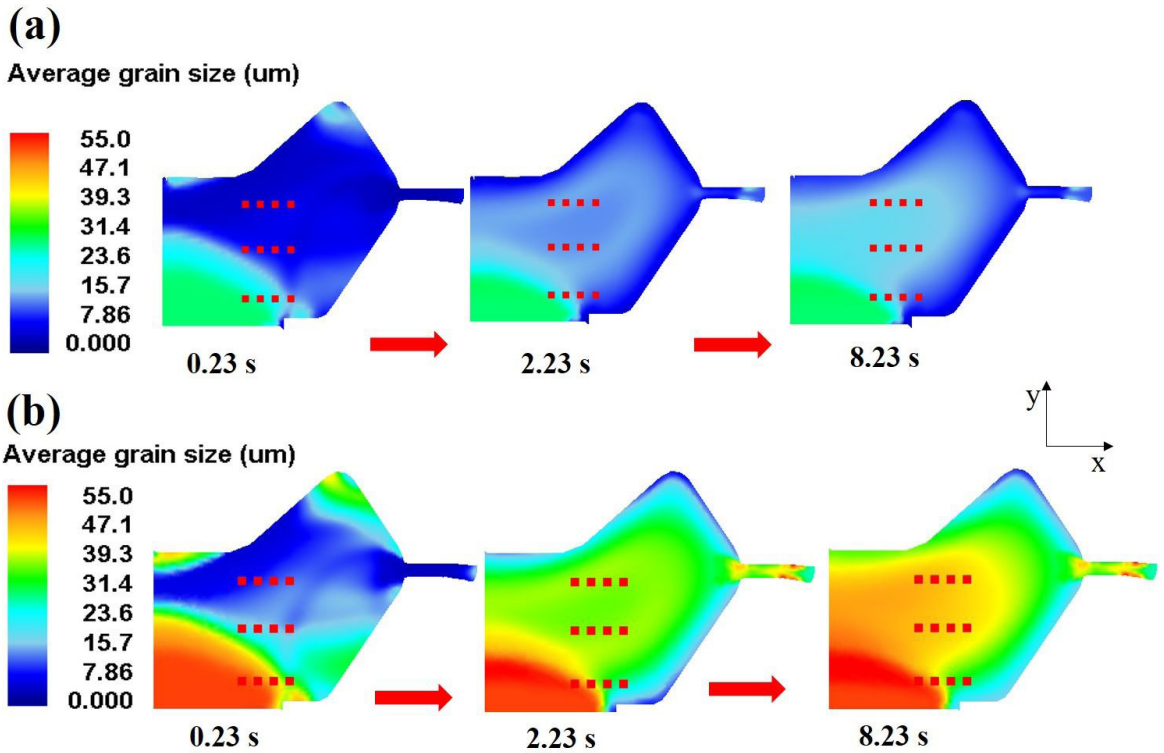

Figure 15. X-Y Plane view of the grain size evolution computed on the tracked points: (a) Forged at 1030 °C, (b) Forged at 1130 °C.

the grain size distribution[18], plastic deformation degree, and temperatures.

Hodgson and Gibbs[30] also stated that high values of *m* are strongly dependent on annealing temperatures and a weak function of the initial recrystallized grain size and holding time. However, in the case of short holding times in closed die forging, the exerted heterogeneous plastic strain distribution, strain rate, and adiabatic heating result in different grain size distribution and recrystallization mechanisms (Figure 11, Figure 12, Figure 13, and Figure 14). Therefore, a constant value of the growth exponent is insufficient to predict the austenite grain growth. Such consideration about this behavior can also be associated with the high-temperature peak condition caused by the adiabatic heating, in which all fine precipitates are dissolved[31].

To distinguish between these parameters with Hillert's theory for ideal growth mechanism[32], we assumed that above 1100 °C, exponent *m* > 4 represents the increase of the growth rate, while *m* between 3-4 would represent a decrease

in growth rate. This makes the magnitude of the collision factor of the atoms decrease in terms of the reactions based on Arrhenius's theory. The modified empirical grain growth exponent values are shown in Table 5.
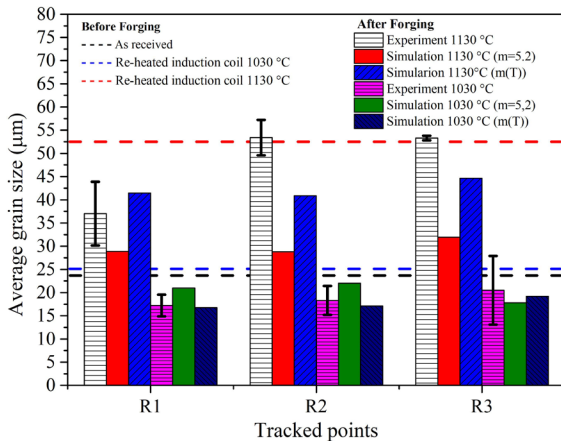
As shown in Figure 15, in the first 2 seconds, most of the heat transfer is between the billet's surface and the lower and upper dies. The pressure of the mechanical system also raises, increasing the temperature in regions R1 and R2 and, therefore, may increase the growth rate for temperatures above 1100 °C.

Figure 16 compares the predicted grain size results with *m* as a constant value and *m* as a function of the temperature in the different regions. Modifying the growth exponent as a temperature function improved the model compared to the constant *m* exponent, closer to the experimental results. The temperature was mainly responsible for the austenitic grain size variation when comparing both cases. However, for the forging done at 1130 °C, the local strain also significantly influenced the grain size variation.

Silveira et al.[8] showed that in a hot forging experiment above 1100 °C at a low strain rate of about 0.17 s⁻¹, the austenitic grain size remained large due to the extended periods the continuous cooling required. In contrast, this work employed high strain rates reaching up to 50 s⁻¹ showing the influence of this parameter when combined with high plastic strain, which resulted in grain refinement when forging above 1100 °C due to adiabatic heating. This can be seen by comparing the R1 and R3 regions. The increase in the strain rate delays the onset of dynamic recrystallization kinetics. i.e., the critical strain ε_c is the trigger for this reaction; therefore, this variation can be explained by the local strain rate gradient.

3.3.3. Mechanical properties response

Experimental results of austenitic grain size were used to validate the accuracy of the numerical simulation. It is essential to remind that, in this present study, the bainitic phase transformation was not modeled. Hence, only the grain size model during hot forging and its influence on mechanical properties is addressed.

Figure 17 shows the experimental austenitic grains in the R2 region and the final microstructure after quenching the forged part at temperatures of 1030 °C (Figure 17a) and 1130 °C (Figure 17b), respectively.

As already mentioned, the dislocation motion is influenced by temperature variation, which is a lower temperature likely decreases the growth rate of the dynamically recrystallized grains. As can be seen, more refined austenitic grain forms when forged at 1030 °C, which shows the importance of controlling the forging temperature of this steel. This grain size variation resulted in different bainitic morphologies in the microstructure after continuous air cooling, as seen at lower magnification in Figures 17b and 17e forged at 1030 °C and 1130 °C, respectively. Visually, it is possible to observe a considerable amount of polygonal ferrite PF at the 1030 °C (Figure 17c) compared to 1130 °C (Figure 17f), which showed less PF fraction in this region and more Lath-like bainite LB.

Figure 16. Local austenitic grain size after industrial hot forging comparing experimental and numerical simulation results.

Table 5. Values of m exponent implemented in DEFORM® computed as a temperature function in non-isothermal conditions after D_{RX}, M_{DRX}, and S_{RX}.

Temperature °C	m-value	$1/m$
1200	5.3	0.1886
1160	4.9	0.2040
1150	4.2	0.2380
1100	3.8	0.2631
1030	3.3	0.3033
1000	3.3	0.3033
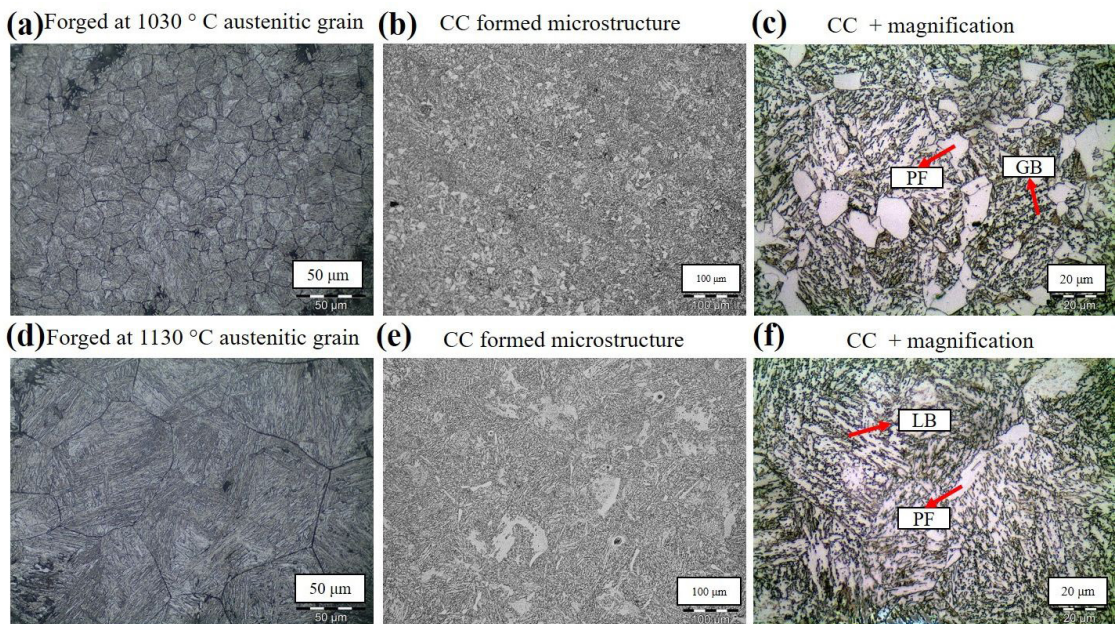
Figure 17. Austenitic grain and continuously cooled microstructure in the R2 region: (a,b) and (c) Forged at 1030 °C, quenched and cooled in calm air; (d,e) and (f) forged at 1130 °C quenched and cooled in calm air.

Austenitic grain refinement increases the amount of ferrite nucleation sites due to the increase in the grain boundary area. The increase in the dislocation density caused by plastic deformation, temperature, and strain rate, are responsible for retained austenite in the microstructure[8,33]. The silicon content in this steel can also be responsible for more carbon enrichment in the retained austenite, which is higher in temperature above 1100 °C[8]. The increase of defects caused by plastic strain increases the number of possible nucleation sites due to the growth of A3 austenite-ferrite transformation[8].

Even at high strain rates, the metallurgical evolution of the ferritic bainite transformation was the same as reported by[6-8]. The temperature significantly influenced the transformations. By forging at 1130 °C, a more significant fraction of the Lath-like bainite can be observed. At 1030 °C, granular bainite rises more.

Finally, the mechanical properties are analyzed. Figure 18a shows the boxplot of the yield YS, and Figure 18b shows the tensile strength US results from the miniaturized tensile tests for the three selected regions of the industrial hot forged component. Figure 19a shows the toughness response of the material to the Charpy impact tests, whereas the elongation (EL) is shown in Figure19b.

The results suggest that the forging temperature was mainly responsible for the increase in the YS (Figure 18a) and US (Figure 18b), where the calculated average stress ratios (YS_{avg}/TU_{avg}) were 0.70 at 1030 °C and 0.68 at 1130 °C. However, by taking the R2 region into account, the plastic strain rate at low temperature also exerted a considerable effect on the YS and TS. This result can be explained through the numerical simulation, which showed that, by the time of forging unloading, the energy accumulated in the R1 region
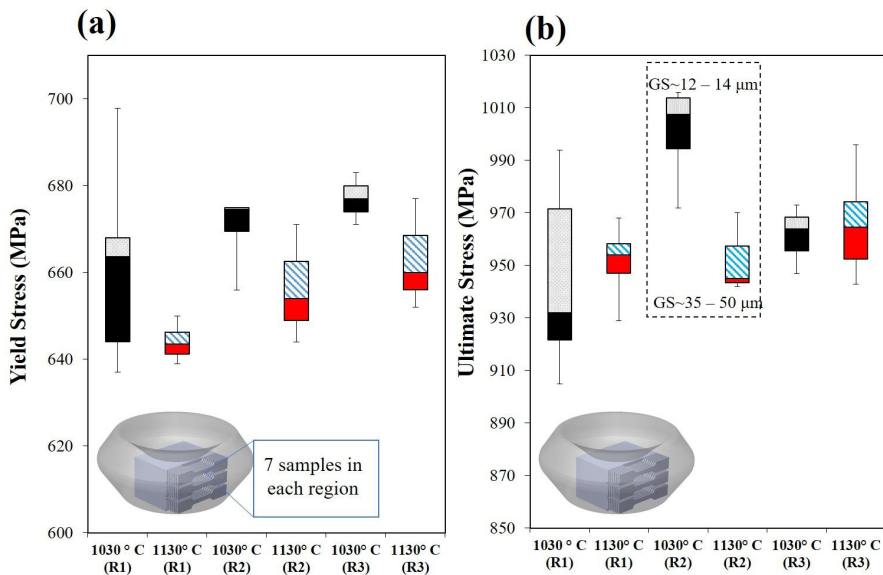

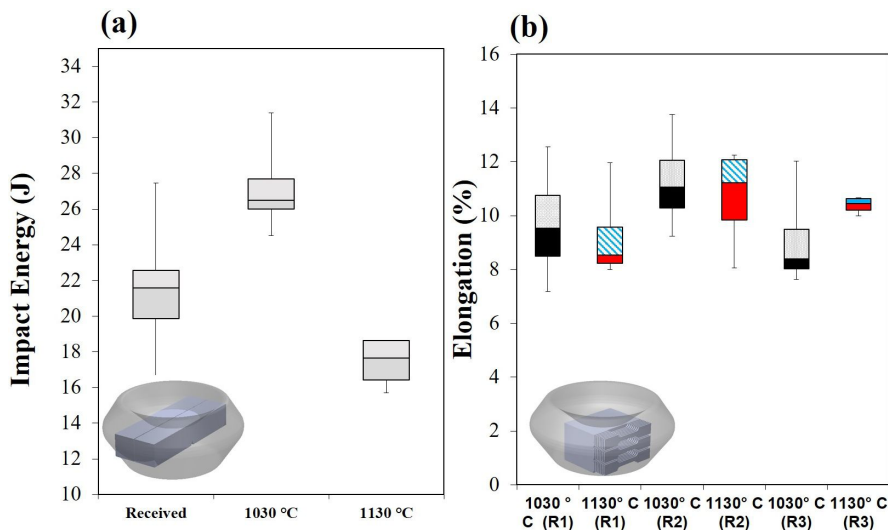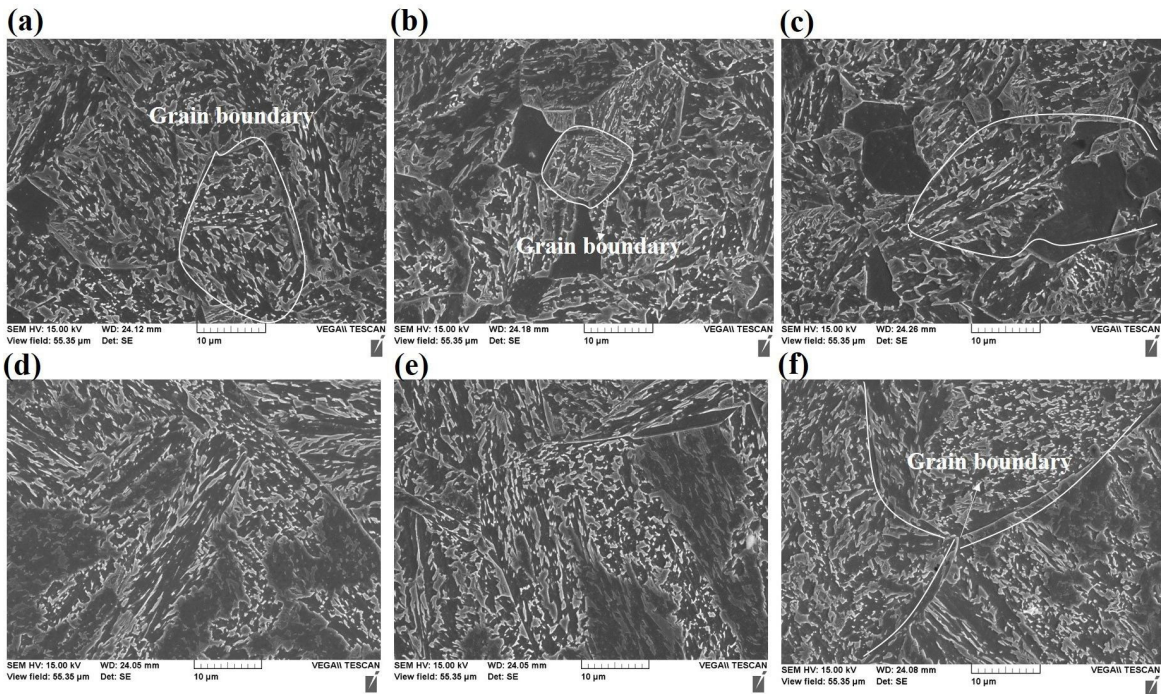**Figure 18.** Boxplot results of the (a) Yield stress YS and (b) Ultimate stress US in MPa.

Figure 19. (a) Impact energy through Charpy- V notch tests; (b) Local Elongation in %.

Numerical and Experimental Study of an Industrial Case for Grain Size Evolution in Bainitic Steel in
Controlled Hot Forging and its Influence on Mechanical Performance

15

Figure 20. SEM results of the micro-tensile specimen regions show the final continuous cooled microstructure of preform gear. (a) R1, (b) R2 and (c) R3 Forged at 1030 °C; (d) R1, (e) R2 and (f) R3 Forged at 1130 °C, respectively.

was greater than R2, which accelerated grain growth due to adiabatic heating, as shown in 2 and Figure 15, respectively.

Figure 20 shows the microstructure from the micro-tensile samples on a magnified scale. The different bainitic morphology revealed by scanning electron microscopy (SEM) in the three regions is shown.

The physical simulations performed by[6,7] with controlled temperature in continuous cooling rate and low strain rate[8] have shown a similar bainitic structure[6-8]. However, in this work, it has been shown that the influence of the temperature variation in high strain rate on the microstructure evolution in an industrial hot forged condition. Figure 20a (R1), Figure 20b (R2), and Figure 20c (R3), forged at 1030 °C, revealed different lengths of grain boundaries compared to the samples forged at 1130 °C (Figure 20d, Figure 20e, and Figure 20f). Finite element analysis showed the local temperature, plastic strain, and strain rate variation for each region of both hot forged conditions. These results encouraged us to interpret that grain boundary changes have been influenced by the synergetic effect in the closed die forging parameters. The temperature variation due to the energy dissipation through plastic strain and strain rate has possibly made the austenite grains in R1 and R2 smaller than R3. At 1030 °C, the grains are more homogeneous and refined than the 1130 °C forging temperature.

The toughness of the component forged at 1030 °C increased compared to the material received and forged at 1130 °C. This result is shown in Figure 19a and confirms the decrease in crystallographic unity (UC), previously shown by the EBSD in Figure 10a. The UC decrease provides a less heterogeneous microstructure package, which could

significantly influence the toughness increase of the bainitic steel, as seen in Figure 11a.

The hot forging at 1030 °C promoted a greater fraction of polygonal ferrite, which, according to[8], resulted in a chemical heterogeneity in the remaining austenite. This phenomenon causes the formation of a higher fraction of martensite in regions with lower concentrations of carbon and alloying elements[34]. This composition heterogeneity is more predominant in R2, which could have resulted in a higher fraction of martensite, which would lead to an increase in strength, as can be seen in Figure 18b and Figure 20b.

4. Conclusion

This work employed the semi-empirical JMAK models to simulate the recrystallization and grain growth after closed die forging for new continuously cooled bainitic steels. The influence of hot forging temperatures on local tensile strength and ductility (toughness) by Charpy V-notch tests was also verified. The following conclusions could be drawn:

- Grain growth exponent, which depends on activation energy, geometric and frequency factors based on the Arrhenius relationship, can vary during the heating and forging steps. Due to the variation of the recrystallized grain size distribution (Figure 11), different exponent values (m) were determined according to temperature. Therefore, after recrystallization, the grain growth results were closer considering the temperature variation.

- From the numerical simulation results, adiabatic heating, caused by high strain rates and plastic deformation, may be responsible for the rapid grain

growth in forging. It was also observed that in hot forging below 1130 °C, the austenite grain size was refined, and abnormal grain growth was absent. This led us to believe that there is no influence on the variation of the exponent *m* at temperatures below 1100 °C.

- The hot forging results below 1130 °C led to higher austenitic grain refinement and no abnormal grain growth. This confirmed previous results in forging tests using a hydraulic press.

- The austenitic grain size favored the formation of different morphologies of bainite at forging temperatures below 1100 °C.

- The localized variations of the bainitic microstructure morphology resulted in different mechanical properties. The temperature of 1030°C in R2 achieved the highest yield strength and the highest ratio between tensile strength and maximum stress, while the toughness could be improved compared to forging at 1130 °C.

- These results showed that, even with a temperature variation of around 100 °C, the control of the temperature forging has a significant impact on the mechanical properties. The numerical simulation was an efficient tool to determine and optimize the austenitic grain evolution.

5. Acknowledgments

6. References

1. Shimanov M, Korpala G, Terzic A, Kawalla R. Bainitic steels, their characteristics and applications. KEM. 2016;684:104-10. https://doi.org/10.4028/www.scientific.net/KEM.684.104.

2. Caballero FG, Capdevila C, Chao J. The microstructure of continuously cooled tough bainitic steels. In: 2nd International Conference of Super-High Strength Steels; 2010 Oct 27-30; Verona, Italy. Proceedings. Verona, Italy: TIB; 2010. p. 10-8.

3. Roelofs H, Hasler S, Urlau U, Lembke MI, Olschewski G. Continuously cooled bainitic steel HSX ® Z12: one decade of experience. In: 4th International Conference on Steels in Cars and Trucks; 2014, Jun 15-19; Braunschweig, Germany. Proceedings. Braunschweig, Germany.

4. Caballero FG, Garcia-Mateo C, Cornide J, Allain S, Puerta J, Crouvizer M, et al. New advanced ultra high strength bainitic steels: ductility and formability (DUCTAFORM) [Internet]. Brussels: European Commission; 2013 [cited 2021 Nov 24]. Available from: https://op.europa.eu/en/publication-detail/-/publication/9f8dc6ba-d882-48da-9b7b-aa8d7f00dd24

5. Lan HF, Du LX, Li Q, Qiu CL, Li JP, Misra RDK. Improvement of strength-toughness combination in austempered low carbon bainitic steel: the key role of refining prior austenite grain size. J Alloys Compd. 2017;710:702-10.

6. Lemos Bevilaqua W, Epp J, Meyer H, Da Silva Rocha A, Roelofs H. In situ investigation of the bainitic transformation from deformed austenite during continuous cooling in a low carbon Mn-Si-Cr-Mo steel. Metall Mater Trans, A Phys Metall Mater Sci. 2020;51(7):3627-37.

7. Hatwig RA, Dong J, Epp J, Rocha A S. Effect of compressive deformations on the final microstructure of a low carbon high silicon bainitic steel thermomechanically processed. Mater Res. 2021;24(1):1-7.

8. Silveira ACF, Bevilaqua WL, Dias VW, Castro PJ, Epp J, Rocha AS. Influence of hot forging parameters on a low carbon continuous cooling bainitic steel microstructure. Metals (Basel). 2020;10(5):601. https://doi.org/10.3390/met10050601.

9. Ivaniski TM, de Souza TF, Épp J, Rocha AS. Constitutive modelling of high temperature flow behaviour for a low carbon high silicon bainitic steel. Mater Res. 2020;23(5):e20200264.

10. Jonas JJ, Quelennec X, Jiang L, Martin É. The Avrami kinetics of dynamic recrystallization. Acta Mater. 2009;57(9):2748-56.

11. Irani M, Lim S, Joun M. Experimental and numerical study on the temperature sensitivity of the dynamic recrystallization activation energy and strain rate exponent in the JMAK model. J Mater Res Technol. 2019;8(2):1616-27. https://doi.org/10.1016/j.jmrt.2018.11.007.

12. Razali MK, Joun M. A new approach of predicting dynamic recrystallization using directly a flow stress model and its application to medium Mn steel. J Mater Res Technol. 2021;11(18):81-94. http://dx.doi.org/10.1016/j.jmrt.2021.02.026.

13. Chamanfar A, Chentouf SM, Jahazi M, Lapierre-Boire L-P. Austenite grain growth and hot deformation behavior in a medium carbon low alloy steel. J Mater Res Technol. 2020;9(6):12102-12114. https://doi.org/10.1016/j.jmrt.2020.08.114.

14. Moraes ALI, Balancin O. Numerical simulation of hot closed die forging of a low carbon steel coupled with microstructure evolution. Mater Res. 2015;18(1):92-7.

15. Ivaniski TM, Epp J, Zoch H-W, Da Silva Rocha A. Austenitic grain size prediction in hot forging of a 20mncr5 steel by numerical simulation using the JMAK model for industrial applications. Mater Res. 2019;22(5)

16. Sellars CM, Whiteman JA. Recrystallization and grain growth in hot rolling. Met Sci. 1978;13(3-4):187-94. https://doi.org/10.1179/msc.1979.13.3-4.187.

17. Henke T, Hirt G, Bambach M. Optimization of a closed die forging process to manufacture a gear wheel by the use of a response surface model. Adv Mat Res. 2014;922:254-9.

18. Janssens KGF, Raabe D, Kozeschnik E, Miodownik MA, Nestler B. Computacional materials engineering: an introduction to microstructure evolution. Cambridge: Academic Press; 2007. 359 p.

19. Lin J, Balint D, Pietrzyk M. Microstructure evolution in metal forming processes: modelling and applications. Sawston, Reino Unido: Woodhead Publishing; 2012. p. 67-74.

20. ASTM: American Society for Testing and Materials. ASTM E112. West Conshohocken: ASTM; 2014.

21. Castro PJ, Silveira AC F, Ivaniski TM, Turra CJ, Epp J, Rocha A S. Two-step continuous cooling heat treatment applied in a low carbon bainitic steel. Mater Res. 2021;24(2)

22. Kashaev N, Horstmann M, Ventzke V, Riekehr S, Huber N. Comparative study of mechanical properties using standard and micro-specimens of base materials Inconel 625, Inconel 718 and Ti-6Al-4 v. J Mater Res Technol. 2013;2(1):43-7.

23. ASTM: American Society for Testing and Materials. ASTM E2298. West Conshohocken: ASTM; 2018

24. Vasilyev AA, Sokolov SF, Kolbasnikov NG, Sokolov DF. Effect of alloying on the self-diffusion activation energy in γ-iron. Phys Solid State. 2011;53(11):2194-200.

Numerical and Experimental Study of an Industrial Case for Grain Size Evolution in Bainitic Steel in
Controlled Hot Forging and its Influence on Mechanical Performance

17

25. Guo-Zheng Q, Yang W, Ying-Ying L, Jie Z. Effect of temperatures and strain rates on the average size of grains refined by dynamic recrystallization for as-extruded 42CrMo steel. Mater Res. 2013;16(5):1092-105.

26. Li X, Ma X, Subramanian SV, Shang C. EBSD characterization of secondary microcracks in the heat affected zone of a X100 pipeline steel weld joint. Int J Fract. 2015;193(2):131-9.

27. Białobrzeska B, Konat Ł, Jasiński R. The influence of austenite grain size on the mechanical properties of low-alloy steel with boron. Metals (Basel). 2017;7(1):1-20.

28. Cho SH, Kang KB, Jonas JJ. Dynamic, static and metadynamic recrystallization of a Nb-microalloyed steel. ISIJ Int. 2001;41(1):63-9.

29. Jiang H, Dong J, Zhang M, Yao Z. A study on the effect of strain rate on the dynamic recrystallization mechanism of alloy 617B. Metall Mater Trans, A Phys Metall Mater Sci. 2016;47(10):5071-87.

30. Hodgson PD, Gibbs RK. A Mathematical model to predict hot rolled C-Mn and microalloyed the mechanical properties of steels. ISIJ Int. 1992;32(12):329-38.

31. Banerjee K, Militzer M, Perez M, Wang X. Nonisothermal austenite grain growth kinetics in a microalloyed x80 linepipe steel. Metall Mater Trans, A Phys Metall Mater Sci. 2010;41(12):3161-72.

32. Hillert M. On the theory of normal and abnormal grain growth. Acta Metall. 1965;13:227.

33. Aranda MM, Kim B, Rementeria R, Capdevila C, De Andrés CG. Effect of prior austenite grain size on pearlite transformation in A hypoeuctectoid Fe-C-Mn steel. Metall Mater Trans, A Phys Metall Mater Sci. 2014;45(4):1778-86.

34. Lambert A, Lambert A, Drillet J, Gourgues AF, Sturel T, Pineau A. Microstructure of martensite–austenite constituents in heat affected zones of high strength low alloy steel welds in relation to toughness properties. Sci Technol Weld Join. 2000;5(3):168-73. http://dx.doi.org/10.1179/136217100101538164.